J. Fluid Mech. (2014), *vol.* 744, *pp.* 169–182. © Cambridge University Press 2014
doi:10.1017/jfm.2014.70

Thermal transpiration flow through a single rectangular channel

Hiroki Yamaguchi[1,†], Marcos Rojas-Cárdenas[2], Pierre Perrier[2], Irina Graur[2] and Tomohide Niimi[1]

[1]Department of Micro-Nano Systems Engineering, Nagoya University, Furo-cho, Chikusa, Nagoya, Aichi 464-8603, Japan

[2]IUSTI, UMR 7343, CNRS, Aix-Marseille University, 13013 Marseille, France

(Received 24 June 2013; revised 5 December 2013; accepted 28 January 2014; first published online 11 March 2014)

A thermal transpiration flow through a single rectangular micro-channel was studied experimentally for various gas species, including all rare gases, in order to investigate the influence of gas species on the flow properties. The final equilibrium flow characteristics and relaxation time of the pressure variation were evaluated as functions of the rarefaction parameter. The thermal molecular pressure difference was well fitted by the log-normal distribution function, and its magnitude was found to be strongly dependent on the gas species: a larger pressure difference was obtained for molecules of smaller diameter. However, for the thermal molecular pressure ratio and the thermal molecular pressure exponent, which are dimensionless quantities, the dependence on the gas species was negligible. The relaxation time of the pressure variation was well normalized by the characteristic time of the system. The influence of the geometry was evaluated by comparing the present results, obtained for the case of a rectangular channel, with already published data obtained for the case of a circular cross-section tube. The comparison showed that these two geometrical configurations influence the fluid flow in equal manner, if appropriate geometrical parameters are used for their representation.

Key words: micro-/nano-fluid dynamics, non-continuum effects, rarefied gas flow

1. Introduction

Thermal transpiration (thermal creep) is one of the most interesting and specific phenomena in relatively high-Knudsen-number flows. The Knudsen number is defined as the ratio of the molecular mean free path λ to a characteristic length of the system $\mathcal{L}$, i.e. $Kn = \lambda/\mathcal{L}$. This phenomenon occurs when a temperature gradient exists along a channel wall; then the flow is induced in the gradient direction, from the cold side towards the hot side of a channel. The thermal transpiration flow was originally studied by Reynolds (1879) and Maxwell (1879). Later, Knudsen proposed the concept of a molecular compressor (Knudsen 1910*a*,*b*), nowadays known as the Knudsen compressor, which can be used as a pump, too.

† Email address for correspondence: hiroki@nagoya-u.jp

https://doi.org/10.1017/jfm.2014.70 Published online by Cambridge University Press

In recent times, as a result of the rapid development of micro-electro-mechanical systems (MEMS), the phenomenon of thermal transpiration has become topical. Owing to the small characteristic lengths of the devices, gas flows in MEMS are classified as high-Knudsen-number flows even in the case of devices functioning at atmospheric pressure. Therefore, since the micro-manufacturing techniques have reached a large degree of precision, it has become possible to implement thermal transpiration in new-generation scaled-down devices.

One interesting application of the thermal transpiration phenomenon at the micro-scale is the Knudsen compressor/pump. This device has attracted attention as a possible candidate in order to generate a stable fluid flow in MEMS. Since the motion is brought about only by a temperature difference, it does not need the implementation of moving parts, which is a significant advantage for miniaturization. A recent improved version of the Knudsen pump was developed by Vargo and Muntz (2001) and Gupta, An & Gianchandani (2012). In addition, it was used for a micro-scale gas chromatography application by Liu *et al.* (2011) and for a gas separation application by Sugimoto and Hibino (2012).

Furthermore, thermal transpiration can induce parasitic effects, too. The phenomenon has to be taken into account in the thermal management of micro-devices that operate with several heat sources. Since the temperature gradient is enough to launch this phenomenon, an undesired thermal transpiration flow may easily appear inside and around these devices, which may affect their performance. Moreover, creeping flows can occur in vacuum equipment, for the case of pipes that are subjected to temperature inequalities and/or for the case of pressure sensors that operate at a temperature different from that of the fluid flow. In both cases, the measurements of pressure can be compromised and, therefore, a non-realistic determination of the fluid flow can occur. When thermal transpiration occurs, precise information on the real temperature distribution along the device is thus very important.

Experimental investigation on the thermal transpiration for a circular cross-section tube geometry has been carried out (Porodnov, Kulev & Tuchevetov 1978; Rojas-Cárdenas *et al.* 2011, 2012, 2013). However, the rectangular cross-section micro-channel is also widely used in micro-devices but has not been investigated yet. Therefore, data on the parameters that characterize the thermal transpiration in a rectangular channel is urgently required for further understanding of the phenomenon and for improving the fluid dynamic performance in micro-devices and in vacuum equipment.

In this article, the thermal transpiration flow through a single channel with a rectangular cross-section is studied for various gas species. We employed five rare (noble) gases (helium, neon, argon, krypton and xenon) and nitrogen to evaluate the influence of different molecular properties on the thermal transpiration flow. This flow was investigated as a function of the rarefaction parameter δ, which is inversely proportional to the Knudsen number. The conditions for δ ranged from 0.7 up to 80 depending on the gas species, which corresponds to the rarefaction range from the transitional to the slip flow regime. The thermal transpiration flow dependence on the gas species was shown by evaluating three common parameters for the final equilibrium characteristics: the thermal molecular pressure difference (TPD), which is the pressure difference between the hot side and the cold side; the thermal molecular pressure ratio (TPR), which is cold side to hot side pressure ratio; and the thermal molecular pressure exponent (γ), which is the exponent of the temperature ratio when related to the pressure ratio. To investigate the evolution of the mass flow rate to the final equilibrium state, the relaxation time τ, which is strongly related to the

https://doi.org/10.1017/jfm.2014.70 Published online by Cambridge University Press

pressure variation rate, was also discussed. The effect of geometry was investigated by comparing the present results with those obtained for a channel with a circular cross-section, which were extracted from Rojas-Cárdenas *et al.* (2011, 2013).

2. Experimental method

2.1. *Experimental apparatus*

A schematic image of the experimental set-up is shown in figure 1. The micro-channel had a rectangular cross-section with dimensions: height $H = 0.22 \pm 0.01$ mm, width $W = 6$ mm, and length $L = 73$ mm. The channel was grooved on a plate and covered by a flat plate. The plates were made of poly(ether ether ketone) (PEEK), whose thermal conductivity is low, 0.25 W m^{-1} K^{-1}. The advantage of this system is that the channel characteristics, such as material, geometry and dimensions, are easily interchangeable. However, we used a single geometry with a single material in order to study the effect of the gas species on the phenomenon. To realize a temperature gradient along the micro-channel, two blocks with gas reservoirs inside were placed vertically at each end of the channel. The two blocks were made of stainless steel (1.4301), whose temperatures were controlled by an electrical heater for the hot side and circulating water for the cold side, respectively. The micro-channel and the blocks were fabricated in the Institute for Micro Process Engineering (IMVT), Karlsruhe Institute of Technology (KIT), Germany. The pressure was measured at each reservoir by a high-speed response in time (30 ms) capacitance diaphragm gauge (CDG) (Inficon CDG045D (hot side), CDG025D (cold side)). The measurement accuracy for the pressure gauges were 0.15 % and 0.2 % for the hot and the cold side, respectively. The absolute pressure was measured by a CDG at the hot side, and the zero point of the CDG at the cold side was set equal to that of the hot side. There was a small difference in temperature between the reservoirs and the CDGs, and a possible parasitic thermal transpiration flow between the reservoir and the CDG for each side was found to be very small by using the semi-empirical formula (Takaishi and Sensui 1963). The temperature of each block was monitored by a K-type thermocouple (TC) placed on the outside of the blocks, and it was maintained constant during the measurement. However, there might be a small discrepancy between the monitored temperature and that at the channel wall. The hot and the cold reservoirs were connected not only by the micro-channel, but also by a tube with a large diameter compared to the micro-channel, forming a circuit, as in figure 1. A micro-valve (Parker Hannifin) was inserted in the large-diameter tube connection to capture the developed stationary thermal transpiration flow at the beginning of each experiment. The voltage applied to the micro-valve was monitored at 300 Hz to determine a precise closing time. The data from the CDGs and the TCs and the voltage of the micro-valve were captured by a data acquisition system (DAQ) (National Instruments). The test section was also connected to a gas supply and a vacuum pump to control the pressure conditions.

2.2. *Measurement procedure*

To explain the experimental procedure, a typical example of the measured pressure variations with time profiles for the cold and the hot sides for the whole duration of one run are shown in figure 2. The measurement procedure was as follows. Before the measurement, the whole system was evacuated for a long time, and the temperatures of the hot and the cold sides were set and controlled to a certain value.

https://doi.org/10.1017/jfm.2014.70 Published online by Cambridge University Press

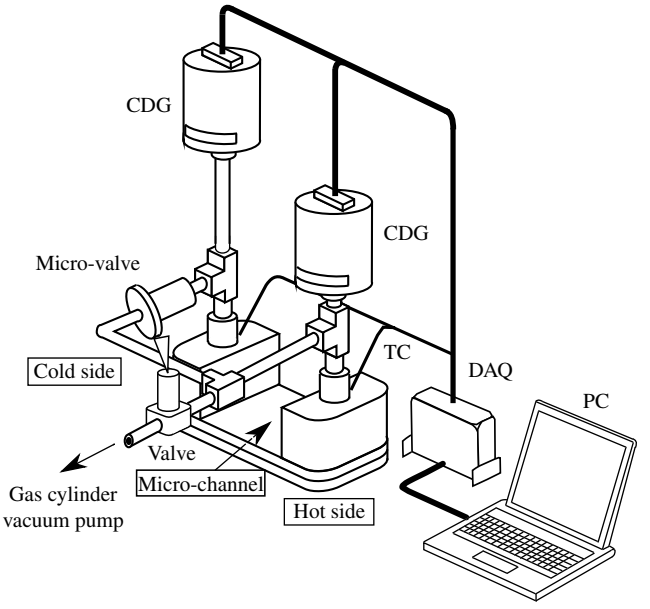


FIGURE 1. Schematic image of experimental apparatus. Pressures for hot and cold sides were measured by capacitance manometers (CDGs). Temperatures were measured by thermocouples (TCs). Data were recorded by a data acquisition system (DAQ).

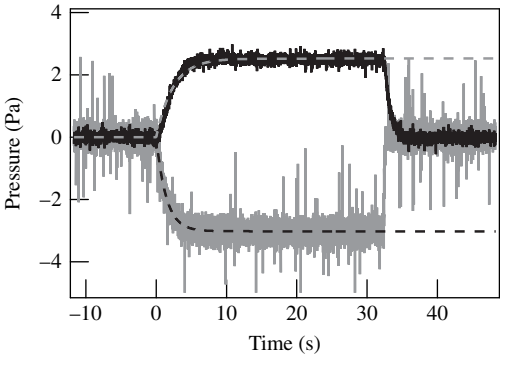


FIGURE 2. A typical example of the pressure profile variation in time for the cold $(p_c(t) - p_i)$ and the hot $(p_h(t) - p_i)$ sides for helium with initial pressure p_i of 466 Pa. Black solid line is pressure of the hot side and grey solid line is that of the cold side. Broken lines are fitted curves by equation (2.1). The pressure variation due to leakages are subtracted from measured values.

The temperature of each side was kept constant during the whole procedure. First, the pressure of the flow circuit was set to a certain condition, and then the line to the gas supply and the vacuum pump was disconnected by closing a bellows-sealed valve. At this moment, the pressures of both sides were equal due to the circuit connected by the large-diameter tube. After a certain period needed to stabilize pressure variations due to the closing of the bellows-sealed valve, the micro-valve was closed too. The pressure started to vary due to the thermal transpiration flow

https://doi.org/10.1017/jfm.2014.70 Published online by Cambridge University Press

from the cold to the hot side. The closing of the micro-valve was monitored by an applied voltage, and the moment, time $t=0$, was decided from this monitoring signal. Since the pressures of the two sides varied differently according to the thermal transpiration flow, a pressure-driven backflow was induced, and then these flows tended to reach equilibrium. After the pressures of the two reservoirs reached their final equilibrium state, the micro-valve was opened again to confirm the pressure equality after the measurement, accomplished by connecting the tube with a large diameter, and by checking the leakage rate throughout the measurement. The leakage rate was calculated from the pressure variation before closing and after opening the micro-valve, and it was checked to be small enough compared to the thermal transpiration flow rate. The pressure variation due to leakage was subtracted from the experimental pressure data to investigate only the thermal transpiration flow.

From figure 2, it is clear that the pressures for both sides are equal to the initial pressure p_i before the closing of the micro-valve at time $t=0$, and they gradually change their values from $t=0$ to $t>0$; the pressure decreases in the cold side whereas it increases in the hot side. Then, the pressures reach their final equilibrium states as $p_{h,\infty}$ and $p_{c,\infty}$. The accomplished pressure differences for the cold and the hot sides are not the same due to the difference in volume for each side. Instantly after the opening of the micro-valve, the pressures return to the same initial pressure p_i. A comparison between the speeds of the pressure variation after the closing and the opening of the micro-valve confirms that the diameter of the connecting tubes is large enough.

2.3. *Data analysis*

The temperatures for the hot and the cold reservoirs were fixed to about 346 K and 289 K, respectively. The temperature difference ΔT between the hot and the cold sides of every measurement was in the range 57.9 ± 0.6 K, where twice the standard deviation (2σ) was used as the uncertainty. The initial pressure p_i was varied from 66.66 to 1266 Pa for every gas species.

The measured pressure variations with time until the final equilibrium state in the reservoirs for the hot side $p_h(t)$ and the cold side $p_c(t)$, respectively, were well fitted by exponential functions (Rojas-Cárdenas *et al.* 2011, 2012, 2013) as follows:

$$p_h(t) = p_i + \Delta p_h \left(1 - \exp\left(-\frac{t}{\tau_h}\right)\right), \quad p_c(t) = p_i - \Delta p_c \left(1 - \exp\left(-\frac{t}{\tau_c}\right)\right). \tag{2.1a,b}$$

In the previous expressions, $\Delta p_c = p_i - p_{c,\infty}$ and $\Delta p_h = p_{h,\infty} - p_i$ are the differences between the initial and final pressures in the cold and hot reservoirs, respectively. The fitting parameters τ_h and τ_c represent the relaxation times in the cold and hot reservoirs, respectively, and their behaviour will be discussed in § 3.3.

The thermal transpiration flow was evaluated by three parameters for the final equilibrium characteristics: the thermal molecular pressure difference (TPD), the thermal molecular pressure ratio (TPR) and the thermal molecular pressure exponent (γ):

$$\mathrm{TPD} = p_{h,\infty} - p_{c,\infty} = \Delta p_h + \Delta p_c, \tag{2.2}$$

$$\mathrm{TPR} = \frac{p_{c,\infty}}{p_{h,\infty}}, \tag{2.3}$$

$$\frac{p_{h,\infty}}{p_{c,\infty}} = \left(\frac{T_h}{T_c}\right)^{\gamma}. \tag{2.4}$$

https://doi.org/10.1017/jfm.2014.70 Published online by Cambridge University Press

It is important to note that in the above equations the TPD is a dimensional value, while the TPR and γ are dimensionless values. These parameters were analysed as a function of the rarefaction parameter

$$\delta = \frac{p\mathcal{L}}{\mu v}, \tag{2.5}$$

where

$$v = \sqrt{\frac{2kT}{m}} \tag{2.6}$$

is the most probable molecular velocity, k is the Boltzmann constant, m is the molecular mass, p and T are the gas pressure and temperature, respectively, and $\mathcal{L}$ is the characteristic length of the system, represented here by the channel height H. The variable hard-sphere (VHS) model (Bird 1994) was employed to evaluate the gas viscosity

$$\mu = \mu_{ref}\left(\frac{T}{T_{ref}}\right)^{\omega}, \tag{2.7}$$

where ω is the viscosity index, which depends on the nature of the gas, and $\mu_{ref}(T_{ref})$ is the gas viscosity at temperature $T_{ref} = 273$ K (Bird 1994).

Since the temperatures of the hot and cold sides were different, the mean temperature $T_{av} = (T_h + T_c)/2$ was employed in order to characterize the rarefaction level δ (equation (2.5)) for each experiment. Let us recall that the temperatures T_h and T_c were maintained constant during the whole experimental series. The pressure range that was used in order to perform the experimental campaign was the same for the whole of the experimental series, independently of the gas species used. Therefore, we chose to characterize a single experiment by associating the rarefaction parameter δ with the initial pressure $p = p_i$, where the thermal transpiration flow is stationary, fully developed and not yet perturbed by the subsequent pressure variation with time. Even if the pressure range chosen for the experimental series did not vary as a function of the gas species used, the rarefaction parameter range did. The rarefaction parameter is directly proportional to the gas molecular mass, too, which makes the rarefaction ranges investigated slightly different for every gas species used. By setting the range of the initial pressure p_i between 66.66 and 1266 Pa, the δ range varied from 0.7 to 80 when considering all the gas species used.

3. Results and discussions

3.1. *Thermal molecular pressure difference*

The measured TPD is shown in figure 3 as a function of δ. The TPD had a peak for each gas species at about $\delta_p \sim 5$, which was independent of the gas species used. The peak value of TPD (denoted by TPD_p) strongly depended on the gas species: a lighter molecule (which, at least for monatomic molecules, has a smaller molecular diameter D) gives a larger value of the peak. The profile of TPD against δ was surprisingly well fitted by a log-normal distribution function as

$$\mathrm{TPD} = \mathrm{TPD}_p \exp\left[-\left\{\frac{\ln(\delta/\delta_p)}{s}\right\}^2\right], \tag{3.1}$$

where s is a parameter that represents the width of the distribution in δ.

https://doi.org/10.1017/jfm.2014.70 Published online by Cambridge University Press

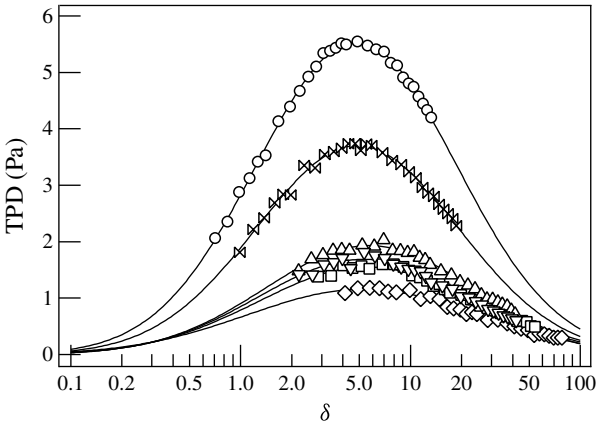


FIGURE 3. The thermal molecular pressure difference (TPD) for rare gases and nitrogen. The symbols represent different gases: ◯, helium; ⋈, neon; ▽, nitrogen; △, argon; □, krypton; ◇, xenon. The solid lines correspond to the fitting curve according to (3.1).

The obtained peak pressure difference TPD_p was investigated using different gas species. The molecular mass m has often been employed to explain empirically the dependence of the flow characteristics on the gas species. We proposed here, in addition to the molecular mass m, to use also the molecular diameter D, defined in the frame of the VHS model (Bird 1994), to seek a better explanation. The data of the TPD_p as a function of the molecular mass and the molecular diameter were fitted and are represented in figure 4. The slopes of the best-fitted lines were -0.45 and -1.73, respectively. However, from a physical point of view, it is known that the most probable molecular speed v (equation (2.6)) is inversely proportional to the square root of the molecular mass and that the collision cross-section is proportional to the square of the molecular diameter. Therefore, we plotted the lines with slopes -0.5 and -2 for the inverse dependence of the TPD_p on the square root of the molecular mass in figure 4(a) and on the square of the molecular diameter in figure 4(b). Error bars estimated by the 95 % confidence interval for the fitting parameter TPD_p are also shown in figure 4. The fitting curves are in reasonably good agreement with the measured TPD_p; however, it seems that the fitting with the square of the molecular diameter represents the measured values better. A new series of measurements on a gas species whose molecular diameter shows a different relation to the molecular mass, such as a polyatomic molecule, is needed for a further discussion.

3.2. *Thermal molecular pressure ratio and exponent*

The TPR and γ are shown in figure 5 also as a function of δ. In the present study, the temperatures T_c and T_h were the same for all measurements; thus, γ can be expressed by TPR as

$$\gamma = \frac{\ln\left(p_{h,\infty}/p_{c,\infty}\right)}{\ln\left(T_h/T_c\right)} \propto \ln\frac{p_{h,\infty}}{p_{c,\infty}} = -\ln \mathrm{TPR}. \tag{3.2}$$

Therefore, the two plots are mirror images of each other. Since the TPR and γ are dimensionless values, their dependences on the gas species are less pronounced, in contrast to the case of TPD. The TPR asymptotically increases to unity for δ values

https://doi.org/10.1017/jfm.2014.70 Published online by Cambridge University Press

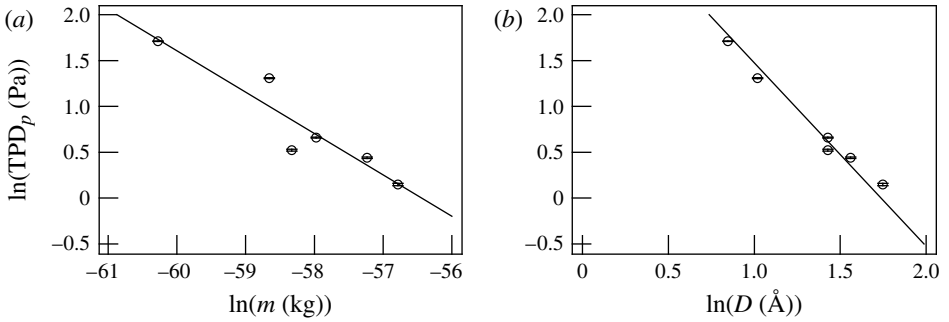


FIGURE 4. Double logarithmic plot for the peak pressure difference TPD_p (Pa) for all gas species as a function of (*a*) the molecular mass (kg) (the solid line is the fitting curve $\mathrm{TPD} = f(1/\sqrt{m})$) and (*b*) the molecular diameter (Å) (the solid line is the fitting curve $\mathrm{TPD} = f(1/D^2)$). Error bars were estimated by the 95 % confidence interval for the fitting parameter TPD_p.

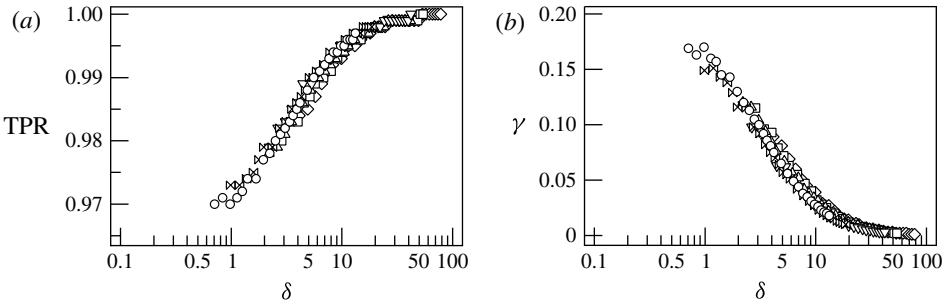


FIGURE 5. (*a*) The thermal molecular pressure ratio (TPR) and (*b*) the thermal molecular pressure exponent (γ) for rare gases and nitrogen plotted against the rarefaction parameter δ. The symbols represent: ◯, helium; ⋈, neon; ▽, nitrogen; △, argon; □, krypton; ◊, xenon.

tending to the hydrodynamic regime. This is due to the fact that, in the continuum regime, the viscous forces of the fluid flow attenuate the final pressure difference achieved by means of thermal transpiration resulting in TPR = 1. The thermal molecular pressure exponent γ increases with decreasing δ, i.e. from the transitional to the near free molecular flow regime. It should be noted that the obtained values of γ are much smaller than the theoretical value of 0.5, predicted initially by Reynolds (1879). However, they are close to the values reported previously in Porodnov *et al.* (1978) and Rojas-Cárdenas *et al.* (2012, 2013).

It is clear from figure 5 that TPR and γ depend on gas species very slightly, in contrast to the case of TPD. This tendency can be explained partially by the fact that both quantities, TPR and γ, are of a dimensionless nature; thus, various characteristic parameters of the gas are smoothed, and the dependence upon the gas species is less pronounced. The specificity of each gas does not intervene more than through gas–surface interaction. However, it is noteworthy that the effect of the gas nature on the TPR and γ is weaker than that found in other works (Porodnov *et al.* 1978; Rojas-Cárdenas *et al.* 2012, 2013). The reason for this difference may be found in the particular properties of the surface used here (roughness, chemical nature): note

https://doi.org/10.1017/jfm.2014.70 Published online by Cambridge University Press

that such smoothing of the gas specific interaction with a surface has previously been shown in other cases (Hadj Nacer *et al.* 2014).

3.3. *Relaxation time*

The relaxation times for the hot and the cold sides, τ_h and τ_c, were employed as a parameter to represent transient flow characteristics (see (2.1)). The pressure variation rate, which is the time derivative of the pressure variation with time, was expressed as follows for the cold and hot sides, respectively:

$$\frac{\mathrm{d}p_h(t)}{\mathrm{d}t} = \frac{\Delta p_h}{\tau_h}\exp\left(-\frac{t}{\tau_h}\right), \quad \frac{\mathrm{d}p_c(t)}{\mathrm{d}t} = -\frac{\Delta p_c}{\tau_c}\exp\left(-\frac{t}{\tau_c}\right). \tag{3.3}$$

Furthermore, if we were to compute the mass flow rate induced by thermal transpiration, the constant-volume technique as modified by Rojas-Cárdenas *et al.* (2012, 2013) could be applied. In the case of considering a reservoir with constant volume and constant temperature, and by assuming that the pressure variations inside the volume were small (Arkilic, Breuer & Schmidt 2001; Ewart *et al.* 2007; Yamaguchi *et al.* 2011), the mass flow rate $\dot{M}$ could be written as (Rojas-Cárdenas *et al.* 2012, 2013)

$$\dot{M} = \frac{\mathrm{d}}{\mathrm{d}t}\left(\frac{mV}{kT}p\right) = \frac{mV}{kT}\frac{\mathrm{d}p}{\mathrm{d}t}. \tag{3.4}$$

Comparing (3.3) and (3.4), it is clear that the pressure variation rate is related to the mass flow rate, which becomes inversely proportional to the relaxation time. This expression represents at any time the mass flow rate entering the cold side reservoir or leaving the hot side reservoir. In precise conditions, where the same pressure has been stabilized in both reservoirs, and when the junction of these reservoirs through the large-diameter tube was closed at time $t = 0$ (see §§ 2.1 and 2.2), equation (3.4) also gives the stationary mass flow rate through the micro-tube.

The relaxation times for the hot and the cold side were strongly correlated due to the conservation of mass inside the system. Therefore, the relaxation time was investigated only for the cold side (τ_c).

The relaxation time τ_c is shown in figure 6(*a*). This relaxation time decreases with increase in δ and it depends strongly on the gas species: τ_c is smaller for lighter gas species. The relaxation time is a dimensional value and it could be normalized by the characteristic time t^c defined by

$$t^c = \frac{L}{v}, \tag{3.5}$$

with the intention of eliminating the dependence on the molecular mass. In (3.5), the most probable flow velocity v (equation (2.6)) was calculated using the temperature of the cold side reservoir, when the relaxation time of the cold side is analysed. The characteristic time t^c could be explained as the time needed for molecules to flow through the channel with the most probable speed. The normalized results are shown in figure 6(*b*). It is clearly shown that the relaxation time can be well normalized by the characteristic time, and that it becomes independent of the gas species. The normalized relaxation time was well fitted by the logarithm of the rarefaction parameter as

$$\frac{\tau_c}{t^c} = -A\ln(\delta/B), \tag{3.6}$$

https://doi.org/10.1017/jfm.2014.70 Published online by Cambridge University Press

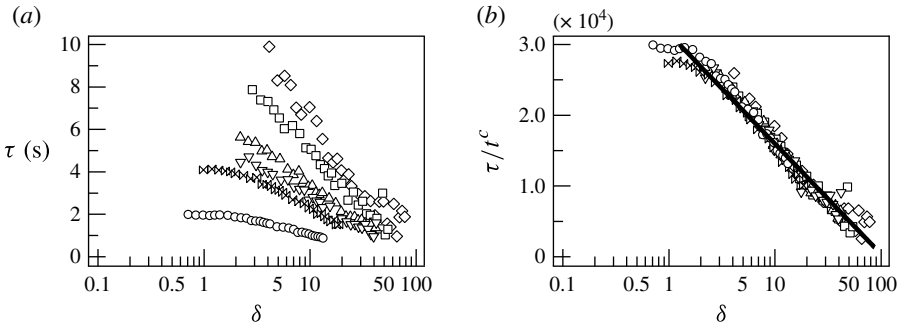


FIGURE 6. The relaxation time for the cold side (τ_c) (*a*) in dimensional form for every gas species and (*b*) in dimensionless form, normalized by the characteristic time t^c (equation (3.5)). The symbols represent: ◯, helium; ⋈, neon; ▽, nitrogen; △, argon; □, krypton; ◇, xenon. The solid line in panel (*b*) corresponds to the fitting curve according to (3.6).

where the coefficients A and B were obtained by a least-squares fitting and are equal to 6.77×10^3 and 1.06×10^2, respectively. We can note that this estimated relation can be applied only when $\delta \leqslant B$ because the relaxation time has to be necessarily positive; nevertheless, this condition does not restrict the use of any of the data obtained in the experimental campaign, since our rarefaction working range is $\delta = 0.7$ to 80.

Furthermore, by using (3.3) and (3.4), let us consider the mass flow rate $\dot{M}_c$ leaving the cold side reservoir at a time t sufficiently close to the stationary final stage (precisely for $t/\tau_c > 1$), which is usually considered as a superposition of the thermal transpiration flow and an associated Poiseuille counterflow. We note then that (3.6) qualitatively corresponds to a drastic decrease of $\dot{M}_c$ with increase in δ. Correspondingly, that would also mean that an associated Poiseuille counterflow had hardly increased and that the thermal transpiration flow varied slightly with the increase in δ. Moreover, we note that such a Poiseuille flow behaviour is closely consistent with those described for the isothermal stationary Poiseuille flow investigated in Perrier *et al.* (2011). Again, that also suggests a minimal value of the associated Poiseuille counterflow with only a small variation in the thermal transpiration flow at this same δ value, and again we remark that a similar feature was observed for the Poiseuille flow described in Perrier *et al.* (2011). In addition, we can also detect, not by analysing (3.6), but on figure 6(*b*), that the τ_c/t^c parameter reaches a maximal value when δ is around 1. Following the previous relations, we consequently obtain a maximal value for the cold reservoir non-stationary mass flow rate at δ close to 1.

3.4. *Effect of geometry*

To investigate the influence of the channel geometry, the present results for a rectangular micro-channel configuration are compared with previously obtained results that were obtained for the case of a micro-tube configuration (Rojas-Cárdenas *et al.* 2011, 2013). In this comparison, the basic final equilibrium characteristic parameters, such as TPD, TPR and γ, and the relaxation time are employed.

It is important to note that there is a small difference in the experimental conditions between the previous and the present studies: the temperatures for the hot and the cold sides in the previous works were 353.5 and 300 K, respectively. These values are slightly higher but close to the conditions in the present study (see § 2.3); furthermore,

https://doi.org/10.1017/jfm.2014.70 Published online by Cambridge University Press

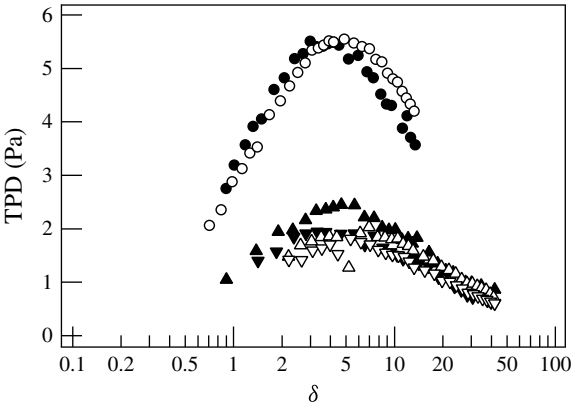


FIGURE 7. The thermal molecular pressure difference (TPD) for rare gases and nitrogen. The symbols represent different gases: ◯, helium; ▽, nitrogen; △, argon. The filled symbols correspond to the results in the previous works (Rojas-Cárdenas *et al.* 2011, 2013).

the temperature difference of about 53.5 K is quite similar to the present study, where this difference is 57.9 K. Therefore, the results are directly comparable with each other.

The TPDs are plotted in figure 7 as a function of δ. The rarefaction parameter δ is calculated from the mean temperature as mentioned above. The choice of the characteristic length of the system in (2.5) is also important. The temperature of the channel was controlled only from one side, while the circular tube was heated from the outside isotropically in the cross-section. Therefore, the characteristic lengths in the present study and in the previous work are selected to be equivalent from the thermal point of view as the channel height H and the tube radius R, respectively. By using an appropriate rarefaction parameter, the TPDs agree well for these two different geometries. There is a good agreement especially in the case of helium, where the pressure difference is large.

The TPR and γ are shown in figure 8 also as a function of δ. These parameters also show similar results for the two geometries considered. They agree well for large δ values. In the case of small δ values, only results for He were available for comparison and they are slightly different in the two studies, when we compare the two geometrical configurations. It should also be noted that the surface materials were not the same in the two experiments: a PEEK surface was investigated in the present study (see § 3.2), while a borosilicate glass surface tube was used in Rojas-Cárdenas *et al.* (2011, 2013). Therefore, as was suggested in § 3.2, this difference may be explained partially by the difference in gas–surface interaction.

The relaxation time τ is inversely proportional to the mass flow rate through a micro-channel at $t = 0$ (see (3.3) and (3.4)), and the mass flow rate is roughly approximated to be proportional to the cross-sectional area. In both experiments, the cross-sectional area A of the micro-channels was different. Therefore, to compare the relaxation times, the expression τA was employed to take into account the difference in the cross-sectional area. The quantity τA is shown in figure 9 also as a function of δ. It is possible to observe that the results for the relaxation time obtained for different geometries and for the same gas species are similar when they are presented in a form that takes into account the cross-sectional area.

https://doi.org/10.1017/jfm.2014.70 Published online by Cambridge University Press

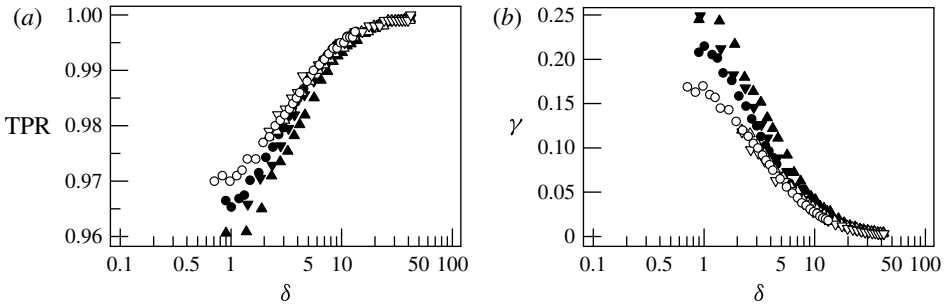


FIGURE 8. (*a*) The thermal molecular pressure ratio (TPR) and (*b*) the thermal molecular pressure exponent (γ) for rare gases and nitrogen plotted against the rarefaction parameter δ. The symbols represent different gases: ◯, helium; ▽, nitrogen; △, argon. The filled symbols correspond to the results in the previous works (Rojas-Cárdenas *et al.* 2011, 2013).

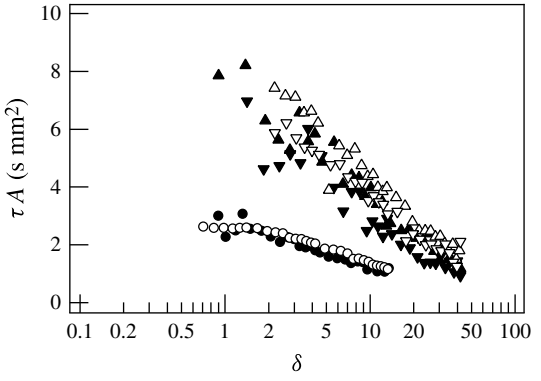


FIGURE 9. The relaxation time τ times the cross-sectional area A for rare gases and nitrogen. The symbols represent different gases: ◯, helium; ▽, nitrogen; △, argon. The filled symbols correspond to the results in the previous works (Rojas-Cárdenas *et al.* 2011, 2013).

It is thus possible to conclude from these results that the influence of geometrical configuration can be taken into account by carefully choosing the appropriate geometrical characteristics of the system. That means also that the present results may be used for the estimation of thermal transpiration flow parameters in other geometries by appropriately choosing the geometrical characteristic parameters.

3.5. *Internal degrees of freedom*

All the characteristics discussed in the present study suggest that the difference in the use of monatomic and diatomic molecules seems to be very small. The temperature difference is quite small, and the range of the Knudsen number (rarefaction parameter) is small. Furthermore, the gas is not far from equilibrium: the internal degrees of freedom are not very excited. These considerations can partially explain the small difference in the obtained results between monatomic and diatomic molecules. However, we employed only nitrogen as a non-monatomic molecule, and a new series of measurements on other polyatomic molecules is needed for a further discussion on

https://doi.org/10.1017/jfm.2014.70 Published online by Cambridge University Press

the influence of the internal degrees of freedom. Note also that the small differences mentioned above may be considered from a more general point of view: the point of view of small differences observed whatever the gas species and discussed at the end of § 3.2.

4. Conclusion

The experimental results for a thermal transpiration flow through a channel of rectangular cross-section are presented for rare gases (helium, neon, argon, krypton and xenon) and nitrogen in order to study the influence of different molecular properties on the flow behaviour. The flow parameters were measured in the transitional and slip flow regimes, where the rarefaction parameter δ varied from 0.7 to 80. One of the final equilibrium flow characteristics, the thermal molecular pressure difference (TPD), strongly depended on the gas species. The TPD profiles for various gases were well explained by a log-normal function. The peak value was obtained for $\delta \sim 5$ for all gases, and the dependence of the peak value TPD_p on gas species seemed to be well explained by the square of the molecular diameter D. The thermal molecular pressure ratio (TPR) and the thermal molecular pressure exponent (γ) showed monotonic variations following δ. The relaxation time τ, which characterizes the pressure variation rate, decreases monotonically with the increase of δ, and it was well normalized by the characteristic time defined by the ratio between the characteristic length of the system and the most probable molecular speed. The influence of the geometry was evaluated by comparing the results obtained for micro-channels of rectangular and circular cross-sections. The influence of geometry configuration was found to be negligible, when the appropriate geometrical characteristics of the system were chosen. Therefore, the TPD, TPR, γ and the relaxation time for an arbitrary channel cross-section may be estimated by using the results obtained here.

Acknowledgements

This study was supported by the Programme 'Creation of Materials, Processes and Systems Provided with New and High Functionality' in the fund 'Institutional Program for Young Researcher Overseas Visit' sponsored by the Japan Society for the Promotion of Science (JSPS). The micro-channel and the blocks were fabricated at the Institute for Micro Process Engineering (IMVT), Karlsruhe Institute of Technology (KIT), Germany, in the framework of the European Community's Seventh Framework Programme (FP7/2007-203 under grant agreement no. 215504). The authors thank Dr Jürgen Brandner for his suggestions in the development of the experimental set-up conception. The authors gratefully acknowledge Dr J. G. Méolans for discussion.

REFERENCES

ARKILIC, E. B., BREUER, K. S. & SCHMIDT, M. A. 2001 Mass flow and tangential momentum accommodation in silicon micromachined channels. *J. Fluid Mech.* **437**, 29–43.

BIRD, G. A. 1994 *Molecular Gas Dynamics and the Direct Simulation of Gas Flows*. Clarendon Press.

EWART, T., PERRIER, P., GRAUR, I. A. & MÉOLANS, J. G. 2007 Mass flow rate measurements in a microchannel, from hydrodynamic to near free molecular regimes. *J. Fluid Mech.* **584**, 337–356.

https://doi.org/10.1017/jfm.2014.70 Published online by Cambridge University Press

GUPTA, N. K., AN, S. & GIANCHANDANI, Y. B. 2012 A Si-micromachined 48-stage Knudsen pump for on-chip vacuum. *J. Micromech. Microengng* **22**, 105026.

HADJ NACER, M., GRAUR, I., PERRIER, P., MÉOLANS, J. G. & WUEST, M. 2014 Gas flow through microtubes with different internal surface coatings. *J. Vac. Sci. Technol.* A **32**, 021601.

KNUDSEN, M. 1910*a* Eine Revision der Gleichgewichtsbedingung der Gase. Thermische Molekularströmung. *Ann. Phys.* **336**, 205–229.

KNUDSEN, M. 1910*b* Thermischer Molekulardruck der Gase in Röhren. *Ann. Phys.* **338**, 1435–1448.

LIU, J., GUPTA, N. K., WISE, K. D., GIANCHANDANI, Y. B. & FAN, X. 2011 Demonstration of motionless Knudsen pump based micro-gas chromatography featuring micro-fabricated columns and on-column detectors. *Lab on a Chip* **11**, 3487–3492.

MAXWELL, J. C. 1879 On stresses in rarefied gases arising from inequalities of temperature. *Phil. Trans. R. Soc. Lond.* **170**, 231–256.

PERRIER, P., GRAUR, I. A., EWART, T. & MÉOLANS, J. G. 2011 Mass flow rate measurements in microtubes: from hydrodynamic to near free molecular regime. *Phys. Fluids* **23**, 042004.

PORODNOV, B. T., KULEV, A. N. & TUCHEVETOV, F. T. 1978 Thermal transpiration in a circular capillary with a small temperature difference. *J. Fluid Mech.* **88**, 609–622.

REYNOLDS, O. 1879 On certain dimensional properties of matter in the gaseous state. Parts I and II. *Phil. Trans. R. Soc. Lond.* **170**, 727–845.

ROJAS-CÁRDENAS, M., GRAUR, I., PERRIER, P. & MÉOLANS, J. G. 2011 Thermal transpiration flow: a circular cross-section microtube submitted to a temperature gradient. *Phys. Fluids* **23**, 031702.

ROJAS-CÁRDENAS, M., GRAUR, I., PERRIER, P. & MÉOLANS, J. G. 2012 An experimental and numerical study of the final zero-flow thermal transpiration stage. *J. Therm. Sci. Technol.* **7**, 437–452.

ROJAS-CÁRDENAS, M., GRAUR, I., PERRIER, P. & MÉOLANS, J. G. 2013 Time-dependent experimental analysis of a termal transpiration rarefied gas flow. *Phys. Fluids* **25**, 072001.

SUGIMOTO, H. & HIBINO, M. 2012 Numerical analysis on gas separator with thermal transpiration in micro channels. In *Rarefied Gas Dynamics* (ed. M. Mareschal & A. Santos), AIP Conf. Proc., vol. 1501, pp. 794–801. American Institute of Physics.

TAKAISHI, T. & SENSUI, Y. 1963 Thermal transpiration effect of hydrogen, rare gases and methane. *Trans. Faraday Soc.* **59**, 2503–2514.

VARGO, S. E. & MUNTZ, E. P. 2001 Initial results from the first MEMS fabricated thermal transpiration-driven vacuum pump. In *Rarefied Gas Dynamics* (ed. T. J. Bartel & M. A. Gallis), AIP Conf. Proc., vol. 585, pp. 502–509. American Institute of Physics.

YAMAGUCHI, H., HANAWA, T., YAMAMOTO, O., MATSUDA, Y., EGAMI, Y. & NIIMI, T. 2011 Experimental measurement on tangential momentum accommodation coefficient in a single microtube. *Microfluid. Nanofluid.* **11**, 57–64.

https://doi.org/10.1017/jfm.2014.70 Published online by Cambridge University Press